Pflügers Arch - Eur J Physiol (2001) 441:506–513
DOI 10.1007/s004240000455

ORIGINAL ARTICLE

Shin Takahashi · Joseph Santos-Sacchi

Non-uniform mapping of stress-induced, motility-related charge movement in the outer hair cell plasma membrane

Received: 21 July 2000 / Received after revision: 24 August 2000 / Accepted: 18 September 2000 / Published online: 7 November 2000

Abstract There is a growing consensus that outer hair cell (OHC) electromotility underlies the mammalian cochlear amplifier. This voltage-dependent motility is mirrored by a gating current, which along with motility can be altered by tension applied to the cell's plasma membrane. We used localized tension application along the length of the OHC to induce gating currents from membrane microdomains; with this information we mapped the distribution of the OHC's sensitivity to membrane stress before and after disrupting the cytoskeleton with intracellular Pronase. Mechanically induced gating currents, which were susceptible to salicylate, lanthanides and turgor pressure, evidenced a bell-shaped distribution that was restricted to the lateral membrane where the electromotile response resides. After Pronase treatment, gating currents remained intact and restricted. These results confirm that the molecular motors are intrinsically and bi-directionally susceptible to voltage and tension, and provide evidence for limited mobility of OHC motors within the cell's lateral membrane.

Keywords Gating charge · Membrane capacitance · Membrane tension · Outer hair cell · Turgor pressure

Introduction

In mammals, the outer hair cell (OHC) provides mechanical feedback into the basilar membrane which enhances auditory sensitivity and frequency resolving power [7, 29]. The likely underlying cellular mechanism is a unique voltage-dependent somatic mechanical response that can be driven at acoustic rates [3, 5, 13, 15, 31, 32]. The mechanical response of the OHC is mirrored by an electrical signature, a motility-related gating current, reminiscent of the gating currents that regulate ion channel conductance [4, 30]. This gating current or charge movement can equivalently be measured as a nonlinear, voltage-dependent capacitance whose cellular location maps to the lateral membrane along the central extent of the cylindrical OHC [19]. This is precisely where the elusive molecular motors responsible for the OHC length change reside [8]. In fact, the lateral membrane harbors, almost exclusively, those sensor/motors that drive somatic motility; voltage-dependent ionic channels are largely absent, and reside in the basal membrane [33]. Beneath the motor-containing lateral membrane lies a well-developed cortical cytoskeleton that maintains the cylindrical shape of the cell [17, 37], and may function to limit the lateral diffusion of intramembranous motors.

One of the most notable features of the OHC is its piezoelectric-like behavior; under voltage clamp, not only do voltage perturbations induce mechanical responses and associated gating currents, but mechanical perturbations of the plasma membrane can induce gating currents as well [4, 14, 21, 22, 30]. Indeed, in the intact sensory epithelium, as a consequence of mechanical coupling through supporting Deiters' cells, the mechanical activity of any one OHC can induce gating currents in adjacent OHCs [41]. The susceptibility of OHC mechanical and electrical activity to membrane stress has been surmised to arise from an action on lateral membrane sensor/motors. Here we utilize this phenomenon to assess the extent of motor activity along the longitudinal axis of the OHC. Our data show that the susceptibility to membrane stress is restricted to the same cellular region that harbors the high density of sensor/motors, confirming the hypothesis that rapid changes in OHC membrane tension induce conformational changes in the molecular sensor/motor elements that are measurable as gating charge movements. Furthermore, the nonuniform distribution that we find provides evidence for limited mobility of OHC motors within the cell's lateral membrane.

J. Santos-Sacchi (✉)
Surgery (Otolaryngology), BML 244,
Yale University School of Medicine, 333 Cedar St.,
New Haven, CT 06510, USA
Tel.: +1-203-7857566

S. Takahashi · J. Santos-Sacchi
Sections of Otolaryngology and Neurobiology,
Yale University School of Medicine,
New Haven, CT 06510, USA

Materials and methods

General preparation

Guinea pigs were overdosed with pentobarbital. The temporal bones were removed and OHCs were isolated from cochleas by gentle pipetting of the isolated top two turns of organ of Corti in Ca-free medium with collagenase (0.3 mg/ml). The cell-enriched supernatant was then transferred to a 700-µl perfusion chamber, and the cells were permitted to settle onto the coverglass bottom. All experiments were performed at room temperature (≅23°C). A Nikon Diaphot inverted microscope with Hoffmann optics was used to observe the cells during electrical recording. A modified Lebovitz medium (NaCl, 142.2 mM; KCl, 5.37 mM; $CaCl_2$, 1.25 mM; $MgCl_2$, 1.48 mM; HEPES, 10 mM; dextrose, 5 mM; adjusted to pH 7.2 with NaOH, and adjusted to 300 mosmol/l with dextrose) was used as the standard perfusion solution.

Electrical recordings

Cells were whole-cell voltage clamped with an Axopatch 200B amplifier (Axon Instruments, Calif., USA). Gigohm seals were obtained at the supra-nuclear region of the OHC membrane prior to whole-cell recording. Patch electrodes had initial resistances of 3–5 MΩ, corresponding to tip sizes of approximately 1–2 µm. The series resistance typically ranged from 8 to 15 MΩ. No series resistance compensation was performed, as this interferes with admittance-based capacitance measures (see below). Pipette solutions were composed of 140 mM CsCl, 10 mM EGTA, 2 mM $MgCl_2$, and 10 mM HEPES (buffered to pH 7.2 with CsOH, and adjusted to 300 mosmol/l with dextrose). In order to evaluate nonlinear capacitive gating currents in the absence of confounding ionic currents, the standard perfusion solution was replaced with an ionic blocking solution following seal formation {NaCl, 100 mM; tetraethylammonium (TEA), 20 mM; CsCl, 20 mM; $CoCl_2$, 2 mM; $MgCl_2$, 1.48 mM; HEPES, 10 mM; dextrose, 5 mM; adjusted to pH 7.2 with NaOH, and adjusted to 300 mosmol/l with dextrose; [19, 30]}. In some cases, the extracellular solution contained 10 mM sodium salicylate (replacing NaCl). Additionally, in some cases intracellular Pronase (500 µg/ml), a wide spectrum proteolytic enzyme, was added to the pipette solution to destroy the cortical cytoskeleton [20, 22, 24, 35]. All chemicals were purchased from Sigma (USA). OHCs were held at 0 mV. Currents were recorded as averages of ten responses. Data collection and analysis were performed with a Window's based whole-cell voltage-clamp program, jClamp (http://www.med.yale.edu/surgery/otolar/santos/jclamp.html), utilizing a Digidata 1200 board (Axon Instruments, Calif., USA). Patch pipette pressure was modified with a syringe connected to the Teflon tubing attached to the patch pipette holder and monitored via a T-connector to a pressure monitor (WPI, Florida, USA). All experiments were video taped.

Membrane capacitance and mechanically evoked gating currents

Voltage-dependent OHC capacitance was measured with a continuous high-resolution two-sine voltage stimulus protocol (10 mV peak at both 390.6 and 781.2 Hz) [35]. Sinusoids were superimposed on voltage ramps.

Restricted regions of the OHC lateral membrane were stressed using a micropipette aspiration technique. This technique has been used extensively to study the mechanical properties of membrane, notably by Evans and associates [10]. In fact, Brownell and colleagues [25] have used it to study the mechanical properties of the OHC lateral membrane through aspiration-evoked deformation.

Aspiration was delivered through a solution-filled glass pipette fitted to a computer-controlled piezoelectric device (PZL, Burleigh Instruments, N.Y., USA) within an in-house-designed pipette holder. The pipette tip was heat polished to a final inner diameter of 2.5 µm. The pipette contained bath solution that interfaced with mineral oil in the fluid-tight, rigid plastic pipette holder. Piezoelectrically driven piston movements within the mineral oil were delivered to the pipette solution. To maintain a tight seal between the pipette tip and the cell membrane, the tip was placed on the cell surface at right angles and slight negative pressure was applied. Tip placement by the micromanipulator was visually observed, and recorded on videotape for later measurement. Membrane deformation was induced by movements of the driver's piston stepped in the negative direction (producing suction) in the range of 200 to 800 nm, controlled by the voltage magnitude delivered to the piezoelectric. For the mapping studies, one fixed voltage was used along the cell length. The spatial pattern of stress delivery along the length of the cell was random; that is, there was no particular path along the cell length that was followed. Additionally, since we found that cell collapse altered the magnitude of mechanically evoked gating currents, we maintained the cylindrical shape of the OHC with small pipette pressures for those cells

Fig. 1A–D On the *left* is a schematic and digitally captured image of isolated outer hair cell illustrating the patch pipette at the supra nuclear region and stimulating pipette. **A** Whole-cell current induced by discrete mechanical stimulation of the lateral plasma membrane. The *Solid line* depicts raw current and the *dotted line* shows the transient current artifact with the stimulating pipette off the cell. **B** Mechanically induced current obtained by subtracting current artifact from the raw current response. **C** As in **B**, except the driving piston in the stimulating pipette was absent, and consequently mechanical stimulation of the membrane was lacking. Under this condition, however, the piezoelectric driver was still activated and transient current artifacts were still generated. **D** Absence of response following the stimulation of the supporting Deiters cell membrane. *Black bar* indicates the duration of mechanical stimulus (see text)

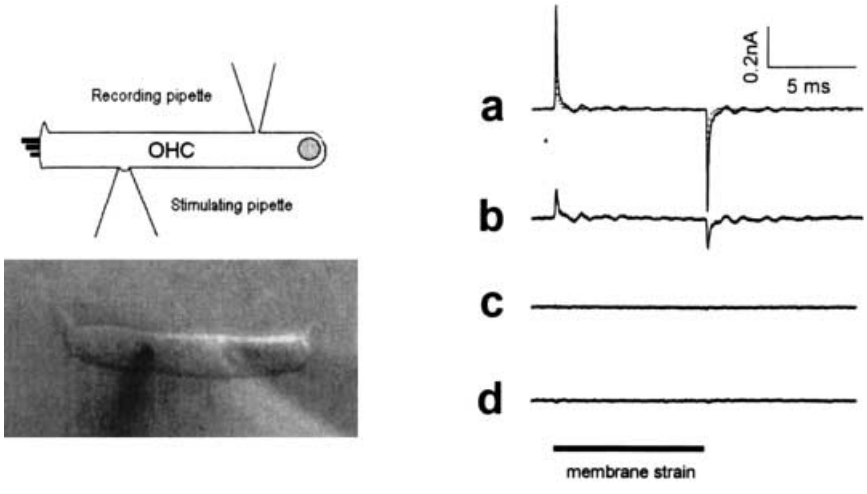

used for mapping experiments (see [22] for details). In some cells, repeat measures were made following mapping, and responses were within 10% of initial ones, indicating that delivery of the stimulus was uniform and repeatable along the length of the cell.

Data are derived from cells in the low frequency region of the organ of Corti, 60–70 μm long. These cells were chosen over shorter, high frequency cells so that the distribution within the lateral membrane could be mapped with increased resolution over our previous electrical amputation method [19]. A particular stimulation location was binned within one of ten equally spaced (6–7 μm) regions along the cell length, providing relative measures of response distribution. Eight of those regions corresponded to the lateral membrane (see Results, and schematic of Fig. 4). If we had chosen smaller cells, the number of regions would have been smaller (given our aspiration pipette size).

Oscillations in the current response were generated by a mechanical resonance in the stimulus delivery system, as has been described previously [14]. The magnitude and frequency of the resonance depended on the piezoelectric device and pipette/membrane seal combination. Resonances around 1 kHz were observed and could be reduced by filtering the command voltage to the piezoelectric. These oscillatory currents are real motor-generated currents, and are differentiated from a concurrent electrical artifact (initial few microseconds – see Results). Such high frequency responses are not unusual since the frequency responsiveness of OHC charge movement extends into the tens of kilohertz range [15]. Membrane currents were quantified by either measuring the RMS value during the extent of the mechanical stimulus, or by integrating the current response over that same period. The latter technique was employed when under some experimental conditions exponentially decaying currents possessed minimal oscillations, so that gating charge estimates could be made. Either measure produced quantitatively similar mapping patterns.

Results

Restricted tension application evokes motility-related gating currents

Under whole-cell voltage clamp with ionic currents blocked, discrete mechanical stimulation of the OHC lateral plasma membrane evokes an initial transient followed by small oscillatory currents (Fig. 1). The piezoelectric-driven aspiration pipette that we use to apply membrane stress contributes a short-lived electrical artifact at the onset (dotted line, Fig. 1A) that is subtracted from the raw response to obtain membrane currents (Fig. 1B). In the absence of the aspiration pipette's driving piston, no membrane currents are elicited (Fig. 1C). Supporting cells do not generate membrane currents when stimulated mechanically (Fig. 1D). Digestion of the subsurface cytoskeleton with intracellular Pronase (500 μg/ml) did not abolish mechanically evoked gating currents, similar to results with voltage-induced charge movement [20].

Further evidence indicating that these discretely generated currents derive from OHC sensor/motors residing in the lateral membrane is obtained from the current's sensitivity to agents that block voltage-induced OHC motility and capacitance. Figure 2A shows that salicylate blocks the mechanically elicited membrane current. Additionally, the currents show a bell-shaped voltage dependence that is expected based on macroscopic methods of mechanical stimulation of the OHC [14, 41]. Pan-

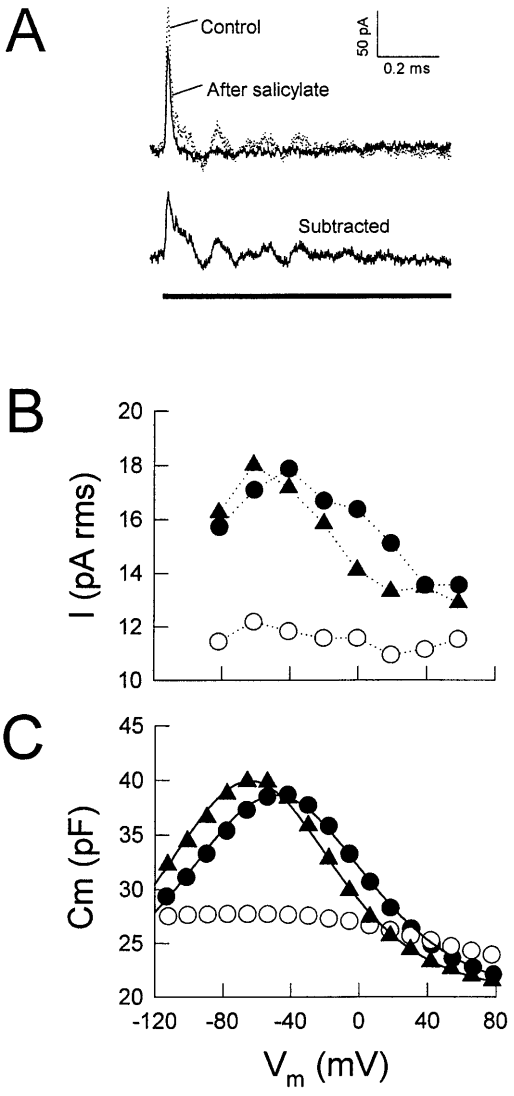

Fig. 2 **A** *Dotted line* illustrates the raw whole-cell current induced by discrete mechanical stimulation of the lateral plasma membrane. The *solid line* is the response after perfusing the cell with 10 mM salicylate. Beneath, the subtracted current represents that current sensitive to salicylate. The *black bar* indicates the duration of mechanical stimulus. **B** Mechanically induced gating current magnitude versus holding membrane potential. *Solid circles* indicate responses before salicylate (10 mM) treatment, *open circles* during salicylate treatment, and *solid triangles* following salicylate washout. **C** Corresponding membrane capacitance as a function of membrane potential. *Symbols* are as in **B**. Fits to the capacitance data were obtained using the following formula:

$$C_m = C_v + C_{\text{lin}} = Q_{\max}\frac{zeb}{kT(1+b)^2} + C_{\text{lin}}$$

$$b = \exp\left(\frac{-ze\left(V_m - V_{\text{pkcm}}\right)}{kT}\right)$$

where $Q_{\max}$ is the maximum nonlinear charge moved, V_{pkcm} is voltage at peak capacitance or half-maximal nonlinear charge transfer, V_{m} is membrane potential, C_{lin} is linear capacitance, z is valence, e is electron charge, k is Boltzmann's constant, and T is absolute temperature. Before salicylate – $Q_{\max}$: 2.56 pC, V_{pkcm}: –63.7, z: 0.78, C_{lin}: 20.4; after washout – $Q_{\max}$: 2.64 pC, V_{pkcm}: –48.8, z: 0.72, C_{lin}: 20.1. The data during salicylate treatment could not be fit reliably

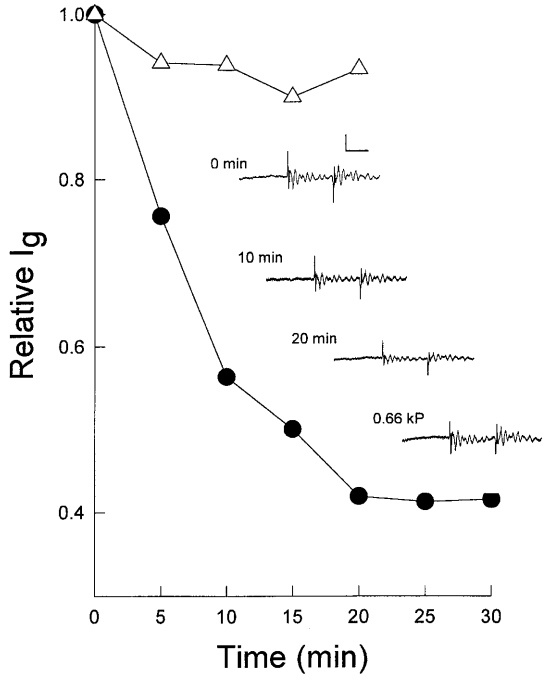

Fig. 3 Mechanically induced gating current magnitude depends on intracellular turgor pressure. Average (n=3) relative gating current magnitude is plotted as a function of time after establishment of whole-cell recording (*filled circles*). The magnitude decreases to less than half of the initial level within 20 min and remains stable after that time. Following stabilization, positive pressure delivered via the patch pipette (≅0.6 kPa) increased the average relative magnitude to 0.81. The *inset* depicts mechanically induced gating currents from a single cell during the course of recording. *Scale* 80 pA, 5 ms. In another five cells (*open triangles*), positive pipette pressure delivered throughout the recording period blocked the decrease in gating current magnitude

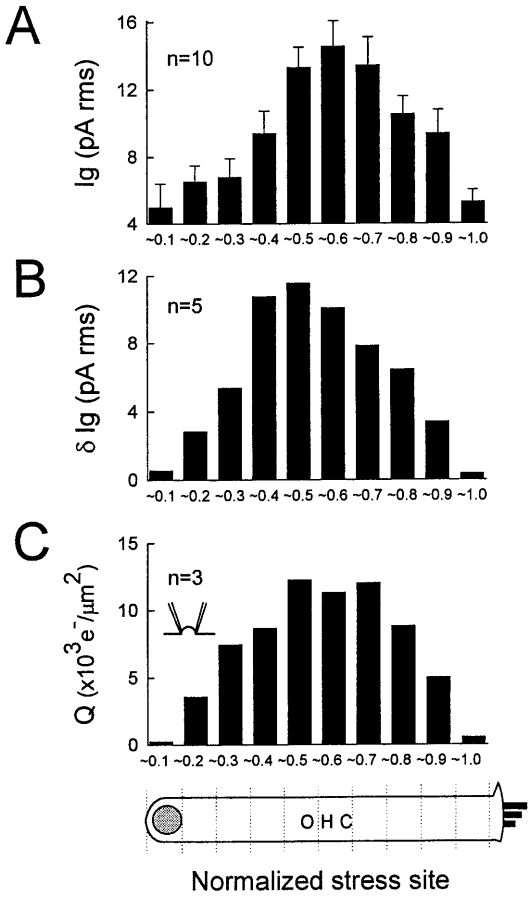

Fig. 4A–C Mechanically induced gating currents are restricted to the lateral membrane of the OHC. **A** Average (±SE; n=10) gating currents as a function of normalized stress site. **B** Five of the cells in **A** were subsequently treated with 10 mM salicylate, and the salicylate-sensitive gating current obtained through subtraction is displayed. Note minimal currents at cell extremes. **C** In three additional cells, where the exponentially decaying gating current dominated the mechanically evoked response, gating charge was determined via integration. Membrane surface area under the stimulating pipette was calculated based on tip diameter and an assumed hemispheric profile. Charge density is similar to that obtained via voltage stimulation paradigms

els B and C of Fig. 2 illustrate the voltage-dependent magnitude of the cell's membrane capacitance and mechanically evoked membrane currents. Each is reversibly reduced by salicylate. The shift in the voltage at peak capacitance (V_{pkcm}) evident after washout is possibly due to a reduction of OHC turgor pressure during the recording. This shift is observable in the current–voltage (I–V) function as well. Gating currents arise from the small area within the orifice of the stimulating pipette; this was confirmed by treatments with lutetium, a known blocker of motility and nonlinear capacitance that works solely on the extracellular aspect of the lateral plasma membrane [23]. When lutetium was placed within the solution of the stimulating pipette nearly all gating current was abolished; however, when lutetium was placed within the bath solution, gating current was little affected, since the blocking agent could not reach the mechanically activated site (data not shown).

Turgor pressure modulates gating current magnitude

The effect of turgor pressure on the mechanically elicited membrane current was studied in detail. It is known that the intracellular pressure of the OHC dissipates following establishment of whole-cell voltage clamp [22]. During that time V_{pkcm} shifts in the negative direction and peak capacitance increases. Figure 3A shows that after the establishment of the whole-cell configuration, mechanically elicited membrane currents (filled circles) decrease in size over a time course similar to the known effects on OHC capacitance [22]. Indeed, simultaneously, V_{pkcm} shifts in the negative direction (data not shown). Applying positive pressure through the patch pipette prevents the decrease in gating current magnitude (open triangles). The current trace insets depict, for a single cell, the decrease in gating current magnitude over the course of 20 min; at that time a positive pressure of 0.66 kPa applied to the patch pipette reestablished the initial magnitude of the mechanically evoked current.

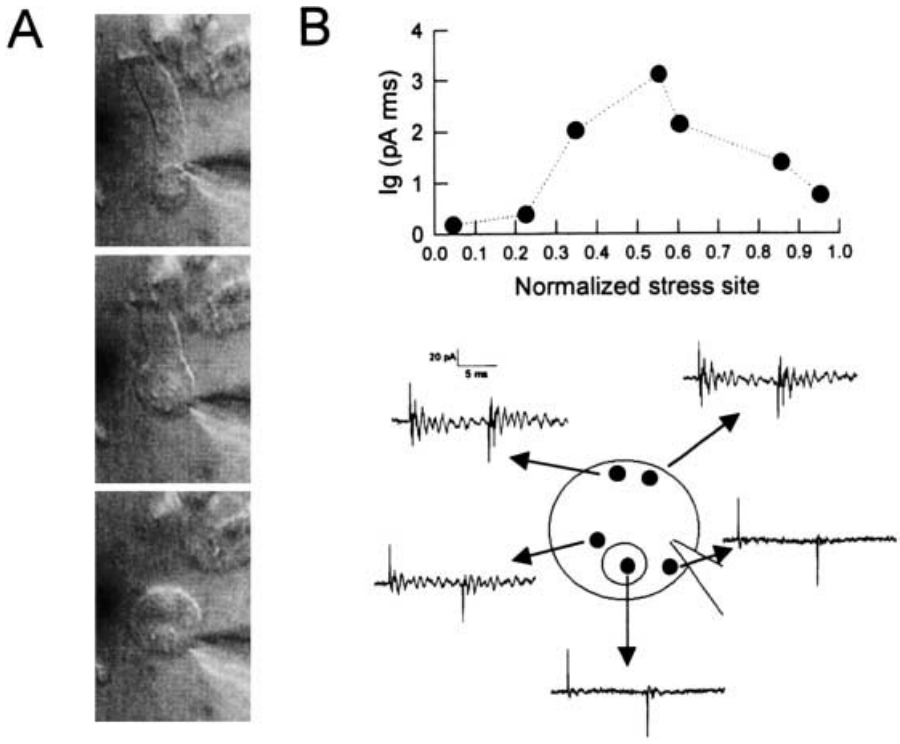

Fig. 5A, B Mechanically induced gating currents remain intact and restricted following cytoskeletal disruption. **A** Digitally captured images of an OHC during recording with Pronase-containing intracellular solution. *Top* – after 9 min; during this time control measurements were made. *Middle* – cell is beginning to form a sphere as the cytoskeleton is disrupted. *Bottom* – after 13 min the cell is fully spherical. Diameter is 24 µm. The cuticular plate is on the underside of the cell. **B** Plot shows restricted gating currents obtained while the cell was still cylindrical. The *bottom schematic* illustrates the cell after the cytoskeleton was destroyed. Gating currents were measured at the regions marked by *filled circles*. Note the absence of response over the nuclear region which was determined from video to correspond to the basal membrane

Tension-induced gating currents map to the lateral membrane in a nonuniform manner

Having confirmed that the membrane aspiration-induced currents derive from OHC motors, we used this method to map the distribution of stress sensitivity within the OHC plasma membrane. Single cells were subjected to multiple discrete mechanical stimulations along the length of the cell. Figure 4A shows the average RMS gating current magnitude along the normalized length of the OHC. The response is clearly largest in the central region of the cell, which corresponds to that region where OHC voltage-dependent capacitance and motility reside [8, 19]. Figure 4B plots the extent of the gating current that is susceptible to salicylate; negligible mechanical sensitivity resides at the extremes of the cell. In three cells it was possible to determine gating charge via integration since an exponentially decaying gating current dominated the mechanically evoked response. In Fig. 4C we plot the average gating charge density from these cases and show that the average density within the central portion of the cell membrane, about 10,000 $e/\mu m^2$, is similar to the charge density obtained by voltage stimulation protocols [19].

Motor distribution is maintained following cytoskeletal disruption

Finally, we examined the effects of destroying the OHC's cortical cytoskeleton on the generation and distribution of stress-induced gating currents. In two cells we were able to perfuse intracellularly with 500 µg/ml Pronase via the patch pipette and map the distribution before and after cytoskeletal disruption. Figure 5 shows an example. Over the course of about 10–15 min, OHCs lose their cylindrical shape and form spheres (Fig. 5A) [20, 22, 24]. In the process, the cortical cytoskeleton is disrupted, leaving free plasma membrane [20]. Before disruption occurred, the cells showed typical distributions of stress-induced gating currents (Fig. 5B, top panels). Following cytoskeletal disruption, gating currents were still evoked by membrane stress, and surprisingly remained restricted in their distribution (Fig. 5B, bottom panels). Having videotaped the experiments, we were able to track and conclusively identify the cell's basal membrane as it changed shape. Over the time course of the experiments (≅20–30 min), lateral diffusion of the molecular motors into the basal plasma membrane did not occur.

Discussion

The OHC is a highly partitioned cell whose sensory activity is augmented by voltage-dependent mechanical activity. OHCs possess a mechano-electrical transduction mechanism within the apical membrane – the stereociliar bundle, and synaptic machinery in the basal membrane. This basic polarization, found in all vertebrate hair cells, has evolved in the OHC, since, additionally, molecular motors responsible for the cell's electro-mechanical transduction are restricted to the lateral membrane [8, 19, 20, 24]. The membrane area comprising the cylindrical cell's lateral membrane can range up to nearly four times that of the combined apical and basal membrane

(e.g., given a 90-μm-long OHC, apical and basal surface area is estimated to be about 750 μm^2, whereas lateral membrane area is about 2700 μm^2).

The OHC lateral plasma membrane displays an unusually dense population of tightly packed 8- to 10-nm particles that probably represent protein motors embedded in the lipid bilayer [12, 16, 24, 34]. Densities up to 6000/μm^2 have been reported. Electrophysiological experiments similarly provide motor density estimates ranging from 2500 to 7500/μm^2 based on voltage-induced gating charge densities from low frequency OHCs [4, 15, 19, 30]. Despite this good correspondence, we have recently shown that the correlation between ultrastructural and electrophysiological estimates of motor density may not hold for high frequency OHCs, where charge density increases more so than membrane particle density [34]. Nevertheless, all estimates clearly indicate that the molecular motors dominate the makeup of the lateral membrane. We now show that the density of mechanically induced charge movement, while not uniform, is similar to those estimates determined through whole-cell voltage stimulation. An average density of 10,000 e-/μm^2 was found, assuming a hemispherical insertion of the membrane into the aspiration pipette. Oghalai et al. [25] have shown that upon slight suction, this type of membrane deformation is expected with an aspiration pipette of our size. Thus, the co-localization of voltage- and mechanical-sensitive charge movement to the lateral plasma membrane that we report here strongly suggests that we are observing intrinsic piezoelectric-like activity of integral membrane motors. That is, voltage and mechanical sensitivity are features of one molecular entity – the motor, and independent of cytoskeletal requirements, since cytoskeletal disruption with Pronase leaves charge movement intact.

The nonuniform distribution of stress sensitivity along the lateral membrane may arise from a true motor distribution pattern or regional differences in the efficacy of mechanical stimulation due, for example, to membrane stiffness gradients along the cell length. It is clear from the turgor results that changes in the mechanical properties of the membrane can influence the magnitude of charge movements, yet it is not obvious from ultrastructural studies that the lateral wall structure harbors such longitudinal mechanical gradients [28]. However, it is clear that abrupt mechanical changes probably arise at the apical and basal terminal borders of the subsurface cytoskeleton and cisternae that lie beneath the lateral plasma membrane. Nevertheless, the changes in charge density are clearly more gradual. Previously, we had mapped the distribution of voltage-induced charge movement using an electrical amputation technique [19]. In order to evaluate our data that were admittedly limited in spatial resolution we modeled the motor density as evenly distributed along the lateral membrane, and concluded that the apical and basal poles of the OHC were devoid of sensor / motors. While our present data confirm the virtual absence of motors in the apical and basal poles, it appears that a uniform distribution is unlikely. This is corroborated to some extent by the findings of Zajic and Schacht [40], who showed that in response to K depolarization mechanical responses in the middle of the OHC are larger than at its apical and basal regions. We conclude that the nonuniform distribution of motors is real and must be an expression of restricted lateral mobility within the plane of the cell's plasma membrane.

The OHC's cortical cytoskeleton is extensive; structural similarities have been found between it and the peripheral cytoskeleton of other cell types, including muscle cells and red blood cells [11, 17, 24, 37]. In the red blood cell, band 3 membrane proteins are restricted in their lateral movements by interactions with the subsurface cytoskeleton (see Edidin [9] for review). Agents that disrupt the cytoskeleton can increase lateral mobility by about two orders of magnitude. In the OHC, the cortical cytoskeleton lies beneath that region of the membrane where the dense array of membrane particles resides, and it is possible that interactions with the motors restrict their diffusion to basal and apical compartments of the cell. We have evidence that protein motors are indeed able to diffuse laterally within the lateral membrane itself [36]. Utilizing microdomain photoinactivation of motor charge movements (i.e., voltage-dependent capacitance), we showed that photo exposure of dye marked OHC lateral membrane for extended periods of time irreversibly depleted whole-cell charge movement beyond that expected for an immobile population in the exposed area. Nevertheless, the present data indicate that diffusion of motors into regions normally devoid of motors, viz. the apical and basal regions, does not occur within the time frame of our experiments. For a typical diffusion coefficient of membrane protein untethered by cytoskeleton, e.g., 1 e-9 cm^2/s [2], we might have expected to observe gating charge movements in the basal region after 10–20 min. For example, if we assume that the molecular motors within the Pronase-treated spherical OHC are initially restricted to one hemisphere then the time to redistribute the motors equally within the sphere would be:

$$\tau = r_o^2/2D$$

where r_o is the cell radius, and D is the diffusion coefficient [18]. With r_o=12 μm (Fig. 5A), and D=1e-9 cm^2/s, we obtain τ of about 12 min. Clearly, this redistribution did not occur. In fact, τ is an overestimate since the motors in our treated cells occupy far greater than 50% of the membrane surface area. Furthermore, motors would only need to diffuse a few microns in order to occupy the basal membrane. It is not unusual for mobilities to vary within different membrane microdomains. For example, voltage-gated Na channels in neuronal soma diffuse more readily than in the axon hillock (one to two orders of magnitude difference in diffusion coefficients) [2]. Indeed, there is a barrier to the diffusion of Na channels between the two regions of neuronal membrane. Tethering by ankyrin probably plays a role in clustering Na channels at the axon hillock [43], and, interestingly, Winckler et al. [39] suggest that this type of interaction

between membrane protein and the cytoskeleton provides a diffusion barrier for other membrane proteins in the neuron as well. Our data, however, suggest that this type of cytoskeletal barrier is not acting to limit the diffusion of lateral membrane motors into the basal membrane region. The story may be different for voltage-gated ion channels that are restricted to the basal membrane of the OHC [32]. Though it cannot be dismissed that their clustering relies on cytoskeletal elements, as do Na channels, the highly organized nature of the subsurface cytoskeleton found in the lateral membrane is absent in the basal membrane. One further means of restricting ionic channel movements to the basal membrane could arise from the high density of molecular motors within the lateral membrane, which would effectively provide a barrier to diffusion into the motor region from the basal membrane. Indeed, the high density may also limit lateral diffusion within the lateral membrane itself. Recently, Oghalai et al. [26, 27] have shown that lipid mobility in the lateral membrane is quantitatively similar to that of other cell types but is dependent upon membrane voltage and tension, as might be expected if the state of the molecular motors, in addition to their density, were influential.

The susceptibility of mechanically induced gating currents to salicylate is understandable since the drug is capable of blocking the OHC's voltage-dependent charge movement (or capacitance) within seconds of application [23, 38]; a mechanically induced shift of the charge–voltage (*Q–V*) function along the voltage axis is thought to give rise to mechanically induced gating currents [14, 22, 41]. Indeed, for this reason, the mechanically evoked currents possess a bell-shaped voltage dependency. However, while some common characteristics of mechanically and voltage-evoked gating currents, e.g., block by salicylate and lanthanides, are readily explainable, the effect of cell turgor on mechanically evoked gating current magnitude is not simply explained, and deserves some discussion. OHCs normally possess a positive intracellular pressure that helps maintain the cylindrical shape of the cell [6]. Steady state decreases in OHC turgor pressure cause negative dc shifts of the *Q–V* or capacitance function along the voltage axis until a limiting V_{pkcm}, near –70 mV, is attained [22]. At that point, tension changes have little effect on V_{pkcm}. This phenomenon may play a role in reducing mechanically generated gating currents when the cell is collapsed from its cylindrical shape; however, from our data it appears that mechanically evoked gating currents are reduced in a graded fashion as intracellular pressure is decreased. Even more confounding is the observation that Q_{max} derived from voltage stimulation appears to *decrease* as intracellular pressure is *increased* [14, 22] until, under extreme conditions, charge movement can be blocked substantially [1]. Of course, these findings might suggest an opposite result from what we found. It should be noted, however, that the changes in turgor pressure that we encountered amount to changes of less than 1 kPa, and, within that range, with an intact cytoskeleton, quite small changes in Q_{max} are expected [22]. Finally, it may simply be that the efficacy of a given stimulus delivered to the membrane patch under the stimulating pipette depends on the degree of resting membrane tension. This might occur if membrane deformation or bending were the effective stimulus. In this regard, we have suggested that after cytoskeletal destruction, the membrane is more sensitive to turgor pressure, as though the cytoskeleton were impeding membrane deformation [22]. This is borne out by independent studies on the stiffness of the OHC lateral wall (combination of the plasma membrane, cortical cytoskeleton and subsurface cisternae) [25], where the component stiffness of the lateral membrane was found to be less than that of the combined cytoskeleton and subsurface cisternae. We can also conclude from these data of Oghalai et al. [25] that our small deformations of the intact lateral wall would not have independently stimulated the lateral membrane, in contrast to the case following Pronase treatment.

The co-localization of a bi-directional voltage/mechanical sensitivity to the lateral plasma membrane underscores an intrinsic feedback mechanism that exists not only within single OHCs but also among OHCs residing within the normally functioning organ of Corti [41]. Just as the motor is restricted to one region of the OHC, the cellular expression of the motor is restricted to only one hair cell type in the mammalian sensory epithelium, viz the OHC. Recently, Dallos and coworkers [42] have identified a protein unique to the OHC which when expressed in nonauditory cells bears the mechanical and electrical signatures of the OHC motor. From this discovery, we can expect more detailed examinations and understanding of the mechanisms responsible for the segregation and mobility of this unique protein within the OHC plasma membrane.

Acknowledgements This work was supported by NIH-NIDCD grant DC00273 to J.S.S. We thank Margaret Mazzucco for technical help.

References

1. Adachi M, Iwasa KH (1999) Electrically driven motor in the outer hair cell: effect of a mechanical constraint. Proc Natl Acad Sci USA 96:7244–7249
2. Angelides KJ, Elmer LW, Loftus D, Elson E (1988) Distribution and lateral mobility of voltage-dependent sodium channels in neurons [published erratum appears in *J Cell Biol* 1989 May 108(5): preceding 2001]. J Cell Biol 106:1911–1925
3. Ashmore JF (1987) A fast motile response in guinea-pig outer hair cells: the cellular basis of the cochlear amplifier. J Physiol (Lond) 388:323–347
4. Ashmore JF (1989) Transducer motor coupling in cochlear outer hair cells. In: Kemp D, Wilson JP (eds) Mechanics of hearing. Plenum, New York, pp 107–113
5. Brownell WE, Bader CR, Bertrand D, de Ribaupierre Y (1985) Evoked mechanical responses of isolated cochlear outer hair cells. Science 227:194–196
6. Chertoff ME, Brownell WE (1994) Characterization of cochlear outer hair cell turgor. Am J Physiol 266:C467–C479
7. Dallos P (1996) Overview: cochlear neurobiology. In: Dallos P, Popper A, Fay R (eds) The cochlea. Springer, Berlin Heidelberg New York, pp 1–43

8. Dallos P, Evans BN, Hallworth R (1991) Nature of the motor element in electrokinetic shape changes of cochlear outer hair cells. Nature 350:155–157
9. Edidin M (1987) Rotational and lateral diffusion of membrane proteins and lipids: phenomena and function. Curr Topics Membr Transp 29:91–127
10. Evans EA (1973) New membrane concept applied to the analysis of fluid shear- and micropipette-deformed red blood cells. Biophys J 13:941–954
11. Flock A, Flock B, Ulfendahl M (1986) Mechanisms of movement in outer hair cells and a possible structural basis. Arch Otorhinolaryngol 243:83–90
12. Forge A (1991) Structural features of the lateral walls in mammalian cochlear outer hair cells. Cell Tissue Res 265:473–483
13. Frank G, Hemmert W, Gummer AW (1999) Limiting dynamics of high-frequency electromechanical transduction of outer hair cells. Proc Natl Acad Sci USA 96:4420–4425
14. Gale JE, Ashmore JF (1994) Charge displacement induced by rapid stretch in the basolateral membrane of the guinea-pig outer hair cell. Proc R Soc Lond B Biol Sci 255:243–249
15. Gale JE, Ashmore JF (1997) An intrinsic frequency limit to the cochlear amplifier. Nature 389:63–66
16. Gulley RS, Reese TS (1977) Regional specialization of the hair cell plasmalemma in the organ of Corti. Anat Rec 189: 109–124
17. Holley MC, Ashmore JF (1988) A cytoskeletal spring in cochlear outer hair cells. Nature 335:635–637
18. Huang HW (1973) Mobility and diffusion in the plane of cell membrane. J Theor Biol 40:11-17
19. Huang G, Santos-Sacchi J (1993) Mapping the distribution of the outer hair cell motility voltage sensor by electrical amputation. Biophys J 65:2228–2236
20. Huang G, Santos-Sacchi J (1994) Motility voltage sensor of the outer hair cell resides within the lateral plasma membrane. Proc Natl Acad Sci USA 91:12268–12272
21. Iwasa KH (1993) Effect of stress on the membrane capacitance of the auditory outer hair cell. Biophys J 65:492–498
22. Kakehata S, Santos-Sacchi J (1995) Membrane tension directly shifts voltage dependence of outer hair cell motility and associated gating charge. Biophys J 68:2190–2197
23. Kakehata S, Santos-Sacchi J (1996) Effects of salicylate and lanthanides on outer hair cell motility and associated gating charge. J Neurosci 16:4881–4889
24. Kalinec F, Holley MC, Iwasa KH, Lim DJ, Kachar B (1992) A membrane-based force generation mechanism in auditory sensory cells. Proc Natl Acad Sci USA 89:8671–8675
25. Oghalai JS, Patel AA, Nakagawa T, Brownell WE (1998) Fluorescence-imaged microdeformation of the outer hair cell lateral wall. J Neurosci 18:48–58
26. Oghalai JS, Tran TD, Raphael RM, Nakagawa T, Brownell WE (1999) Transverse and lateral mobility in outer hair cell lateral wall membranes. Hear Res 135:19–28
27. Oghalai JS, Zhao HB, Kutz JW, Brownell WE (2000) Voltage- and tension-dependent lipid mobility in the outer hair cell plasma membrane. Science 287:658–661
28. Pollice PA, Brownell WE (1993) Characterization of the outer hair cell's lateral wall membranes. Hear Res 70:187–196
29. Ruggero MA, Rich NC (1991) Furosemide alters organ of corti mechanics: evidence for feedback of outer hair cells upon the basilar membrane. J Neurosci 11:1057–1067
30. Santos-Sacchi J (1991) Reversible inhibition of voltage-dependent outer hair cell motility and capacitance. J Neurosci 11:3096–3110
31. Santos-Sacchi J (1992) On the frequency limit and phase of outer hair cell motility: effects of the membrane filter. J Neurosci 12:1906–1916
32. Santos-Sacchi J, Dilger JP (1988) Whole cell currents and mechanical responses of isolated outer hair cells. Hear Res 35:143–150
33. Santos-Sacchi J, Huang GJ, Wu M (1997) Mapping the distribution of outer hair cell voltage-dependent conductances by electrical amputation. Biophys J 73 :1424–1429
34. Santos-Sacchi J, Kakehata S, Kikuchi T, Katori Y, Takasaka T (1998) Density of motility-related charge in the outer hair cell of the guinea pig is inversely related to best frequency. Neurosci Lett 256:155–158
35. Santos-Sacchi J, Kakehata S, Takahashi S (1998) Effects of membrane potential on the voltage dependence of motility-related charge in outer hair cells of the guinea-pig. J Physiol (Lond) 510:225–235
36. Santos-Sacchi J, Zhao HB (1999) Green card motors: OHC lateral membrane molecular motors may travel. Midwinter Meeting of the Association for Research in Otolaryngology
37. Tolomeo JA, Steele CR, Holley MC (1996) Mechanical properties of the lateral cortex of mammalian auditory outer hair cells. Biophys J 71:421–429
38. Tunstall MJ, Gale JE, Ashmore JF (1995) Action of salicylate on membrane capacitance of outer hair cells from the guinea-pig cochlea. J Physiol (Lond) 485:739–752
39. Winckler B, Forscher P, Mellman I (1999) A diffusion barrier maintains distribution of membrane proteins in polarized neurons [see comments]. Nature 397:698–701
40. Zajic G, Schacht J (1991) Shape changes in isolated outer hair cells: measurements with attached microspheres. Hear Res 52:407–410
41. Zhao HB, Santos-Sacchi J (1999) Auditory collusion and a coupled couple of outer hair cells. Nature 399:359–362
42. Zheng J, Shen W, He D, Long K, Madison L, Dallos P (2000) Prestin is the motor protein of cochlear outer hair cells. Nature 405:149–155
43. Zhou D, Lambert S, Malen PL, Carpenter S, Boland LM, Bennett V (1998) AnkyrinG is required for clustering of voltage-gated Na channels at axon initial segments and for normal action potential firing. J Cell Biol 143:1295–1304